



## Synthesis and Biological Evaluation of Coumarin Derivatives with Promising Anti-Cancer Activity: Computational Kinase Profiling and Molecular Modeling Analysis

Mahmoud S. Elkotamy <sup>1,\*</sup>, Mohamed A. Abdelrahman <sup>1,2</sup>, Wagdy M. Eldehna <sup>3,\*</sup>, Hatem A. Abdel-Aziz <sup>4</sup>, Sahar M. Abou-Seri <sup>5,\*</sup>



<sup>1</sup> Pharmaceutical Chemistry Department, Faculty of Pharmacy, Egyptian-Russian University, Badr City Cairo 11829, Egypt.

<sup>2</sup> Department of Pharmacy, Kut University College, Al Kut, Wasit, 52001, Iraq.

<sup>3</sup> Department of Pharmaceutical Chemistry, Faculty of Pharmacy, Kafrelsheikh University, Kafrelsheikh, P.O. Box 33516, Egypt

<sup>4</sup> Department of Applied Organic Chemistry, National Research Center, Dokki, Cairo 12622, Egypt.

<sup>5</sup> Department of Pharmaceutical Chemistry, Faculty of Pharmacy, Cairo University, Kasr El-Aini Street, Cairo 11562, Egypt

### Abstract

The growing resistance and toxicity associated with current cancer treatments highlight the urgent need for novel therapeutic agents. In this study, we synthesized a series of pyrazolopyrimidine-coumarin derivatives (**10a-d**) and evaluated their anti-cancer activity using the NCI-60 cell line panel, representing nine cancer types. Among the compounds, **10c** demonstrated the most potent activity, achieving a mean growth inhibition of 50% across the entire cell lines' panel. To investigate its mechanism of action, we performed molecular docking studies against 18 kinases, identifying JAK1 and CDK2 as primary potential targets with binding affinities comparable to the ligands co-crystallized with the PDB protein complexes. Pharmacokinetic and toxicity predictions using ADMETLab 3.0, OSIRIS Property Explorer, and ProTox-III confirmed compound **10c** as a promising drug-like candidate. These findings position **10c** as a potential lead compound for developing next-generation anti-cancer agents. Future efforts will focus on optimizing this scaffold to combat resistance and toxicity, particularly enhancing JAK1 and CDK2 inhibition. This study underscores the potential of coumarin-based derivatives in advancing cancer therapeutics.

**Keywords:** Coumarin; Pyrazolo[1,5-a]pyrimidine; Anti-cancer; Molecular docking.

### 1. Introduction

Cancer constitutes a major global health issue, as indicated by the International Agency for Research on Cancer (IARC), which reported around 19.3 million new cases and nearly 10 million deaths in 2020. Projections suggest an increase to over 28.4 million cases by 2040, attributed to population aging and lifestyle modifications [1]. Despite advancements in early diagnosis and targeted therapies, treatment regimens encounter significant limitations, such as severe side effects, inadequate specificity, and multidrug resistance (MDR), which compromise therapeutic efficacy and elevate cancer recurrence rates [2]. Cancer complexity is heightened by tumor heterogeneity, observed both within individual tumors and among patients, alongside challenges from tumor microenvironments, angiogenesis, and metastasis [3]. The identified factors highlight the necessity for innovative therapeutic strategies, leading researchers to investigate new molecular scaffolds to tackle these challenges [4]. Chemotherapy is a fundamental component of cancer treatment, utilizing more than 100 agents in various single or combination regimens that target cancer cells via multiple mechanisms, including the disruption of DNA replication and the inhibition of dysregulated signal-transduction pathways [5, 6].

Compounds inspired by natural products, especially coumarins, have garnered considerable interest in medicinal chemistry owing to their structural diversity and capacity to influence various biochemical pathways [7]. Coumarin derivatives demonstrate a wide range of anti-cancer activities, encompassing anti-proliferative, anti-angiogenic, and apoptosis-inducing effects, positioning them as promising candidates for drug development [8-10]. Their structural versatility enables optimization for improved target specificity and pharmacokinetic properties, effectively addressing challenges such as MDR and off-target toxicity. These compounds function via various mechanisms, including DNA intercalation that disrupts replication and transcription (**I-II**) [11], inhibition of topoisomerases resulting in DNA damage and apoptosis (**III**) [12], and anti-angiogenic effects through the inhibition of VEGF, which suppresses tumor vascularization (**IV-VI**) [13-15]. They also act as anti-mitotic agents by disrupting microtubule assembly and cell division (**VII-VIII**) [16, 17]. Coumarin derivatives inhibit the PI3K/AKT pathway, which is often dysregulated in cancers, thus reducing proliferation and survival (**IX**) [18]. Compounds that target carbonic anhydrases IX and XII (**X-XI**), which are overexpressed in hypoxic tumor microenvironments, effectively disrupt pH regulation, tumor progression, and metastasis [9, 19]. The diverse mechanisms

\*Corresponding authors: [mahmoudekkotami@gmail.com](mailto:mahmoudekkotami@gmail.com); (Mahmoud S. Elkotamy), [wagdy2000@gmail.com](mailto:wagdy2000@gmail.com); (Wagdy M. Eldehna), [sahar.shaarawy@pharma.cu.edu.eg](mailto:sahar.shaarawy@pharma.cu.edu.eg); (Sahar M. Abou-Seri).

Received date 12 December 2024; Revised date 28 December 2024; Accepted date 29 December 2024

DOI: [10.21608/ejchem.2024.343991.10974](https://doi.org/10.21608/ejchem.2024.343991.10974)

©2025 National Information and Documentation Center (NIDOC)

highlight the potential of coumarins as versatile and efficient anti-cancer agents. (**Figure 1**)

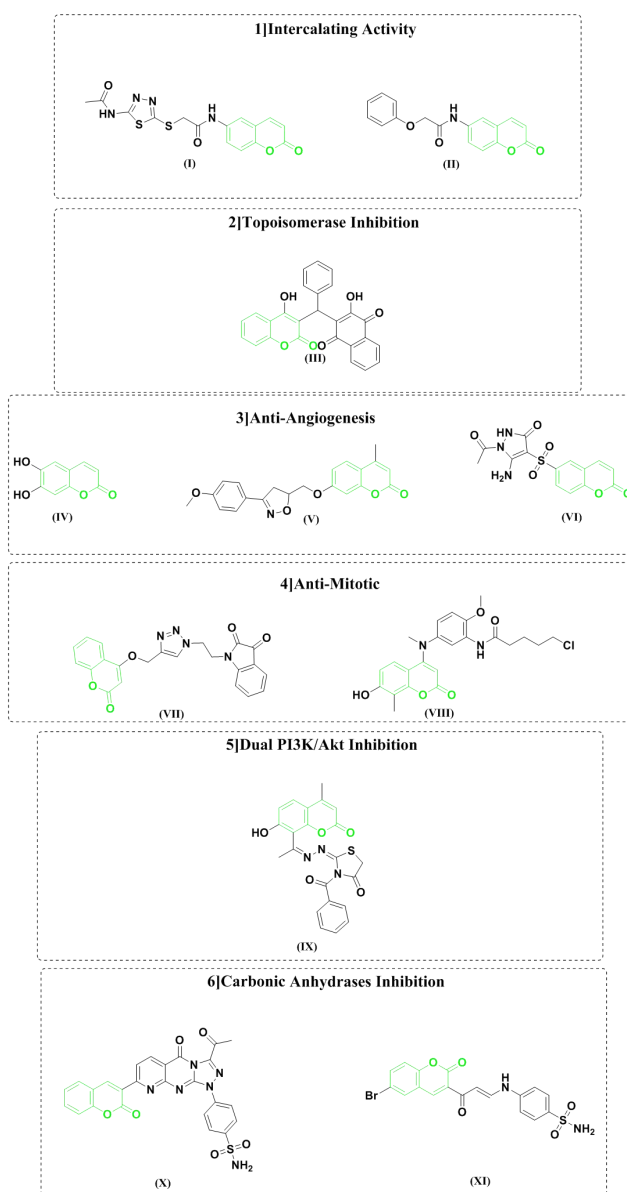


**Figure 1.** Representative examples of the various mechanisms of action that coumarin demonstrates in combating cancer through compounds **I-XI**.

The pyrimidine scaffold has become a crucial structure in developing anti-cancer agents due to its distinctive physicochemical properties and capacity to engage with diverse biological targets [20]. This heterocyclic framework is fundamental in numerous FDA-approved medications and investigational compounds currently in clinical trials (**Figure 2**). Ruxolitinib (**XII**), a pyrimidine-based JAK1/2 inhibitor, is approved for treating myelofibrosis and polycythemia vera, showcasing its effectiveness in addressing cytokine-driven cancers [21]. Tofacitinib (**XIII**) is a significant example, as it is primarily approved for autoimmune disorders but has demonstrated potential in cancer therapies that target the JAK/STAT pathway [22]. Furthermore, the scaffold is integrated into molecules like Baricitinib (**XIV**) [23] and Fedratinib (**XV**) [24], which both focus on JAK-related pathways and are currently under investigation for oncology applications. The versatility of the pyrimidine scaffold also encompasses the inhibition of kinases such as PI3K, CDK, and Aurora kinases, which play a crucial role in tumor progression and survival [25, 26]. The capacity to participate in hydrogen bonding and  $\pi$ - $\pi$  interactions with enzyme active sites improves its potency and selectivity, establishing it as a significant framework for developing next-generation anti-cancer therapeutics. The presence of this scaffold in both approved drugs and advanced clinical candidates highlights its essential role in contemporary oncology drug discovery [27].

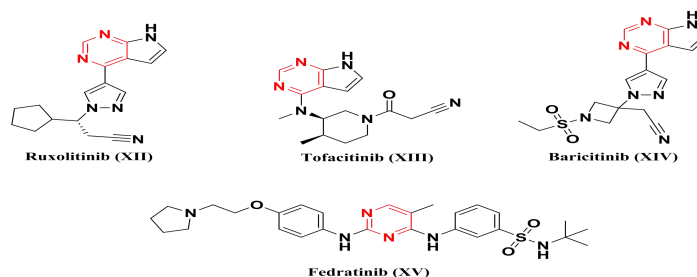


**Figure 2.** Pyrimidine-containing compounds (XII–XV) as cancer combatants, as authorized by the FDA or in clinical trials.

### 1.1. Design rationale

In the current study, the design of the targeted compounds was thoughtfully influenced by our prior research on CAN508 (XVI) [28] as demonstrated by the analogue (XVII) [29] utilizing essential insights to improve their anti-cancer efficacy. Our approach involved the preservation of the pyrazolo[1,5-*a*]pyrimidine scaffold, recognized for its significant kinase inhibitory activity and potential as a versatile backbone in anti-cancer applications. To enhance lipophilicity and potentially improve cellular permeability, we substituted the hydrophilic NH<sub>2</sub> group in the original design with a phenyl group. Additionally, acknowledging the anti-cancer properties of coumarins, we replaced the traditional enaminones in the tail with 3-acetyl coumarin-based enaminone, which offers further advantages, including DNA intercalation, anti-mitotic activity, and the modulation of essential oncogenic pathways. In the diazophenyl head, we incorporated various substitutions with electron-donating and electron-withdrawing groups to systematically examine their effects on electronic distribution and binding interactions, to optimize the compounds' affinity and selectivity for their biological targets. This design incorporates structural modifications enhancing lipophilicity, binding specificity, and pharmacokinetic properties to develop potent and selective anti-cancer agents demonstrating improved therapeutic efficacy (Figure 3).

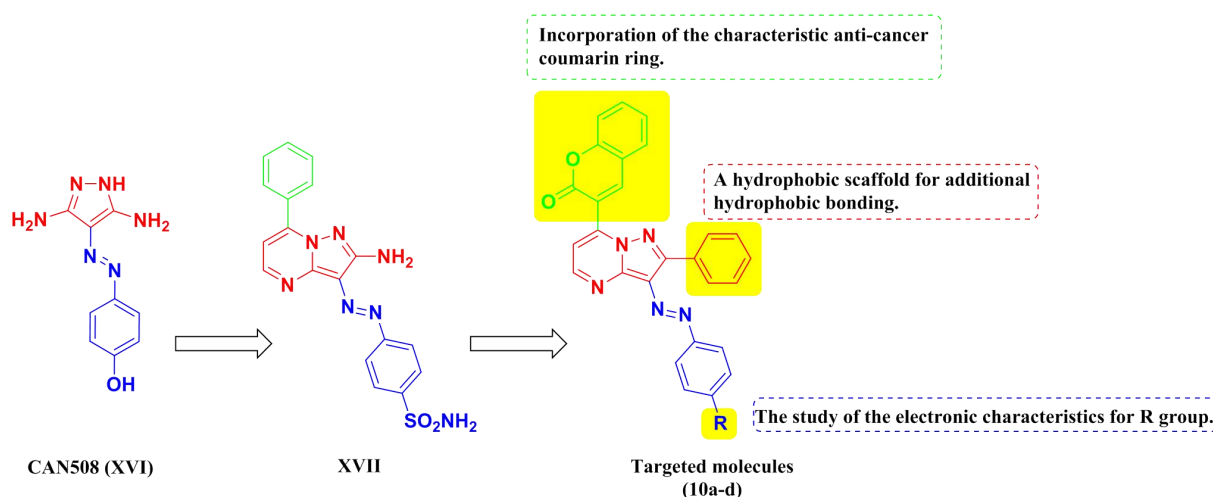


**Figure 3.** The rationale for designing the new targeted molecules 10a-d.

The current investigation into coumarin-based compounds, recognized for their capacity to disrupt critical cancer pathways and tackle existing therapeutic challenges, represents an important avenue for advancing innovative anti-cancer strategies. These initiatives demonstrate the potential to improve patient outcomes and significantly contribute to addressing the global cancer burden by advancing more effective and personalized treatments. The selected molecules (10a-d) will undergo testing on NCI-60 cell line panels to calculate the GI% for each molecule across nine different cancer types. Subsequently, *in-silico* investigations will be performed on the most promising molecule to analyze the molecular modeling related to potential kinases through which these molecules may exert their anti-cancer properties and assess their ADMET profile.

## 2. Experimental

### 2.1. Chemistry

The melting points were determined utilizing an uncorrected Stuart melting point apparatus. The FT-IR 8400S spectrophotometer was employed to obtain infrared spectra. The <sup>1</sup>HNMR spectra were obtained using a Bruker spectrometer operating at 400 MHz. <sup>13</sup>CNMR spectra were recorded in deuterated dimethylsulfoxide (DMSO-*d*<sub>6</sub>) at a frequency of 101 MHz. Chemical shifts (H) are reported relative to TMS, the internal standard. All coupling constant values (*J*) are provided in hertz.

Chemical shifts (C) are reported relative to DMSO- $d_6$  as per internal standards. The abbreviations are as follows: s for singlet, d for doublet, t for triplet, and m for multiplet. Thin layer chromatography (TLC) utilizing silica gel precoated F<sub>254</sub> Merck plates was employed to systematically monitor reaction courses and product mixtures. Elemental analyses were performed at the Regional Center for Microbiology and Biotechnology at Al-Azhar University in Cairo, Egypt. Unless stated otherwise, all solvents and reagents were obtained from commercial sources and utilized without additional purification.

### 2.1.1. General procedure to synthesize the key intermediates (6a-d) and (9)

3-Phenyl-4-(phenyldiazenyl)-1H-pyrazol-5-amine derivatives (6a-d) [30] and coumarin-enaminone derivative (9) [31] were synthesized according to previously reported protocols.

### 2.1.2. General procedures for the synthesis of target coumarins-pyrazolopyrimidine derivatives (10a-d)

3-Phenyl-4-(phenyldiazenyl)-1-pyrazol-5-amine derivatives (6a-d) (2 mmol) were introduced to a hot solution of 3-(3-(dimethylamino)acryloyl)-2H-chromen-2-one (9) (2 mmol) in glacial acetic acid (10 ml). The reaction mixture was stirred and heated under reflux for 8 hours. Subsequently, the reaction mixture was filtered while maintaining elevated temperatures, and the resultant solid was washed with ethanol and recrystallized from an ethanol/DMF solution to yield the desired coumarins (10a-d).

#### 2.1.2.1. 3-(2-Phenyl-3-(phenyldiazenyl)pyrazolo[1,5-a]pyrimidin-7-yl)-2H-chromen-2-one (10a)

Yellow powder (yield 79%), m.p. > 300 °C; IR (KBr,  $\nu$   $\text{cm}^{-1}$ ): 1728 (C=O); <sup>1</sup>H NMR (DMSO- $d_6$ )  $\delta$ ppm: 7.49-7.53 (m, 3H, Ar-H), 7.55 (d, 2H,  $J$  = 7.6 Hz, Ar-H), 7.58-7.62 (m, 4H, Ar-H), 7.64 (d, 1H,  $J$  = 4.4 Hz, Ar-H), 7.84 (d, 2H,  $J$  = 7.2 Hz, Ar-H), 7.94 (d, 1H,  $J$  = 8 Hz, Ar-H), 8.15 (d, 2H,  $J$  = 7.6 Hz, Ar-H), 8.90 (s, 1H, H<sub>4</sub> of coumarin), 8.98 (d, 1H,  $J$  = 4.4 Hz, Ar-H); <sup>13</sup>C NMR (DMSO- $d_6$ )  $\delta$ ppm: 112.95, 116.12, 117.02, 118.61, 122.25, 125.46, 125.78, 129.11, 129.90, 130.11, 130.20, 130.41, 131.91, 134.37, 139.26, 141.62, 143.46, 147.36, 154.12, 154.26, 158.08 (C=O of coumarin); Anal. calcd. for C<sub>27</sub>H<sub>17</sub>N<sub>5</sub>O<sub>2</sub> (443.47): C, 73.13; H, 3.86; N, 15.79. Found: C, 73.27; H, 3.84; N, 15.77.

#### 2.1.2.2. 3-(2-Phenyl-3-(p-tolyldiazenyl)pyrazolo[1,5-a]pyrimidin-7-yl)-2H-chromen-2-one (10b)

Yellow powder (yield 52%), m.p. > 300 °C; IR (KBr,  $\nu$   $\text{cm}^{-1}$ ): 1735 (C=O); <sup>1</sup>H NMR (DMSO- $d_6$ )  $\delta$ ppm: 2.41 (s, 3H, -CH<sub>3</sub>), 7.38 (d, 2H,  $J$  = 8 Hz, Ar-H), 7.50-7.62 (m, 6H, Ar-H), 7.74 (d, 2H,  $J$  = 8 Hz, Ar-H), 7.79 (t, 1H,  $J$  = 8 Hz, Ar-H), 7.93 (d, 1H,  $J$  = 7.6 Hz, Ar-H), 8.14-8.16 (m, 2H, Ar-H), 8.89 (s, 1H, H<sub>4</sub> of coumarin), 8.95 (d, 1H,  $J$  = 4.4 Hz, Ar-H); <sup>13</sup>C NMR (DMSO- $d_6$ )  $\delta$ ppm: 21.45 (-CH<sub>3</sub>), 112.70, 117.01, 118.66, 122.24, 125.21, 125.77, 129.09, 129.85, 130.05, 130.28, 130.40, 131.98, 134.33, 139.28, 140.71, 141.37, 143.73, 145.16, 147.30, 152.16, 153.44, 153.71, 154.33, 157.64 (C=O of coumarin); Anal. calcd. for C<sub>28</sub>H<sub>19</sub>N<sub>5</sub>O<sub>2</sub> (457.49): C, 73.51; H, 4.19; N, 15.31. Found: C, 73.68; H, 4.15; N, 15.34.

#### 2.1.2.3. 3-(3-((4-Fluorophenyl)diazenyl)-2-phenylpyrazolo[1,5-a]pyrimidin-7-yl)-2H-chromen-2-one (10c)

Yellow powder (yield 71%), m.p. > 300 °C; IR (KBr,  $\nu$   $\text{cm}^{-1}$ ): 1732 (C=O); <sup>1</sup>H NMR (DMSO- $d_6$ )  $\delta$ ppm: 7.40 (t, 2H,  $J$  = 8.4 Hz, Ar-H), 7.49-7.56 (m, 4H, Ar-H), 7.59 (d, 1H,  $J$  = 8.4 Hz, Ar-H), 7.64 (d, 1H,  $J$  = 4.4 Hz, Ar-H), 7.80 (t, 1H,  $J$  = 7.6 Hz, Ar-H), 7.89-7.92 (m, 2H, Ar-H), 7.94 (d, 1H,  $J$  = 7.6 Hz, Ar-H), 8.13-8.15 (m, 2H, Ar-H), 8.90 (s, 1H, H<sub>4</sub> of coumarin), 8.98 (d, 1H,  $J$  = 4.8 Hz, Ar-H); <sup>13</sup>C NMR (DMSO- $d_6$ )  $\delta$ ppm: 112.72, 116.69, 116.91, 117.02, 118.60, 124.31, 124.40, 125.11, 125.64, 129.11, 129.90, 130.11, 130.29, 131.87, 134.48, 139.27, 141.63, 147.37, 150.69, 154.01, 154.17, 154.33, 157.78 (C=O of coumarin); Anal. calcd. for C<sub>27</sub>H<sub>16</sub>FN<sub>5</sub>O<sub>2</sub> (461.46): C, 70.28; H, 3.50; N, 15.18. Found: C, 70.21; H, 3.48; N, 15.19.

#### 2.1.2.4. 3-(3-((4-Chlorophenyl)diazenyl)-2-phenylpyrazolo[1,5-a]pyrimidin-7-yl)-2H-chromen-2-one (10d)

Yellow powder (yield 75%), m.p. > 300 °C; IR (KBr,  $\nu$   $\text{cm}^{-1}$ ): 1732 (C=O); <sup>1</sup>H NMR (DMSO- $d_6$ )  $\delta$ ppm: 7.51-7.57 (m, 4H, Ar-H), 7.61 (d, 1H,  $J$  = 8 Hz, Ar-H), 7.65-7.68 (m, 3H, Ar-H), 7.82 (d, 1H,  $J$  = 8 Hz, Ar-H), 7.85 (d, 2H,  $J$  = 8.4 Hz, Ar-H), 7.96 (d, 1H,  $J$  = 8 Hz, Ar-H), 8.14 (d, 2H,  $J$  = 7.6 Hz, Ar-H), 8.92 (s, 1H, H<sub>4</sub> of coumarin), 9.01 (d, 1H,  $J$  = 4.4 Hz, Ar-H); <sup>13</sup>C NMR (DMSO- $d_6$ )  $\delta$ ppm: 113.03, 117.02, 118.58, 123.86, 125.36, 125.77, 129.12, 129.94, 129.98, 130.18, 130.30, 131.95, 134.75, 139.32, 141.69, 147.42, 152.65, 157.71 (C=O of coumarin); Anal. calcd. for C<sub>27</sub>H<sub>16</sub>ClN<sub>5</sub>O<sub>2</sub> (477.91): C, 67.86; H, 3.37; N, 14.65. Found: C, 67.81; H, 3.34; N, 14.62.

## 2.2. Screening anti-proliferative activity against NCI-59 panel

It was completed at the NCI in Bethesda, Maryland, USA, following their regular operating procedure [32].

### 2.3. In-silico investigations

The three platforms utilized for the *in-silico* ADMET investigations were performed on three webservers: ADMETLab 3.0, OSIRIS Property Explorer, and ProTox-III [33-35]. The JAK1 (PDB Code: 3EYG) [36] and CDK2 (PDB Code: 6Q4G) [37] were molecularly modeled following the precise box spacing and detailed protocol outlined in the Supplementary Materials.

## 3. Results and Discussion

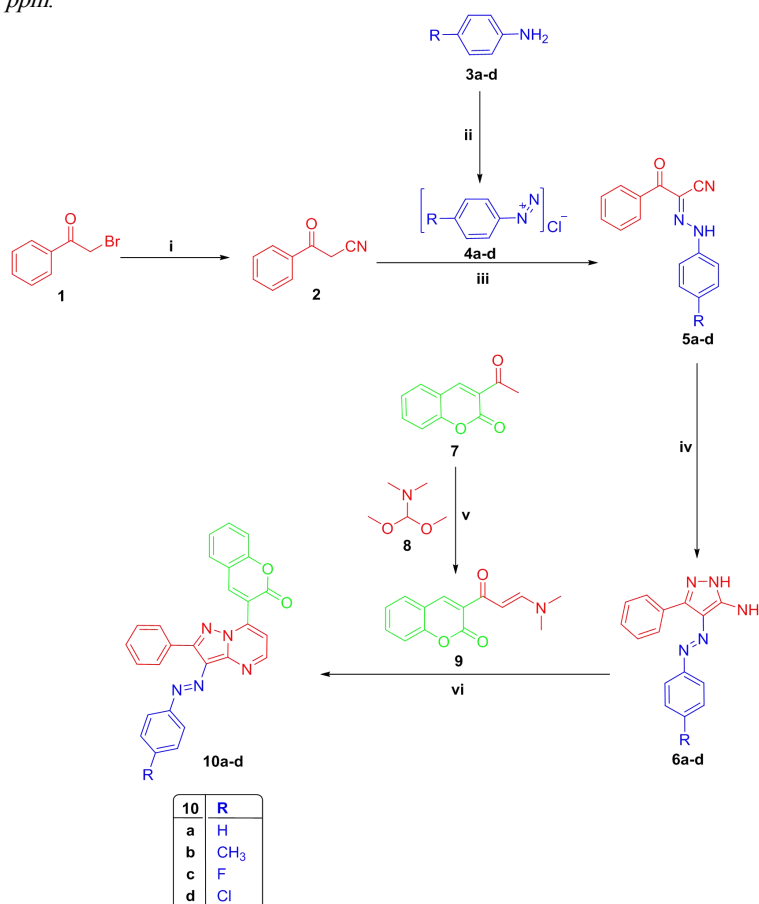
### 3.1. Chemistry

The synthetic pathways utilized to prepare the target coumarin-based analogues (10a-d) are illustrated in Scheme 1. To produce 3-oxo-3-phenylpropanenitrile (2), dissolve phenacyl bromide (1) in ethanol and combine with 3 equimolar potassium

cyanide in water. The reaction mixture is stirred at room temperature to produce 3-oxo-3-phenylpropanenitrile (**2**) [38]. The first key intermediates (**5a-d**) are synthesized by diazotizing different anilines (**3a-d**) to yield the diazonium salt (**4a-d**), which is then coupled on 3-oxo-3-phenylpropanenitrile (**2**) at zero temperature to yield different *N*,2-diphenylacetohydrazonoyl cyanide derivatives (**5a-d**), which are then refluxed in ethanol using hydrazine hydrate to yield the key intermediates. 3-phenyl-4-(phenyldiazenyl)-1*H*-pyrazol-5-amine (**6a-d**) [30].

The enaminone intermediate of coumarin (**9**) is synthesized by solubilizing 3-acetylcoumarin (**7**) in dry xylene, followed by refluxing with DMF-DMA (**8**) to yield the second key intermediate [31]. The concluding step involves refluxing both key intermediates in acetic acid for 8 hours to achieve the desired pyrazolo[1,5-*a*]pyrimidine coumarin-based compounds (**10a-d**). The solid obtained was subsequently washed with ethanol and recrystallized using a mixture of ethanol and DMF to yield the desired coumarins (**10a-d**).

The targeted compounds (**10a-d**) were validated via spectrophotometric analysis. The infrared (IR) charts indicated the presence of the coumarin carbonyl group at approximately 1732  $\text{cm}^{-1}$ . The  $^1\text{H}$ NMR spectra of (**10a-d**) displayed a singlet signal of coumarin-H-4 resonating at approximately 8.90  $\text{ppm}$ . The characteristic peak of the methyl group present in compound (**10b**) was observed at 2.41  $\text{ppm}$ . The  $^{13}\text{C}$ NMR spectra validated the presence of the methyl group, evidenced by a resonating peak at 21.45  $\text{ppm}$ .



**Scheme 1. Reagents and conditions:** **i.** Potassium cyanide,  $\text{H}_2\text{O}/\text{EtOH}$  room temperature, 12 h; **ii.**  $\text{NaNO}_2$ ,  $\text{HCl}$ , 0-5  $^\circ\text{C}$ , 30 min; **iii.**  $\text{EtOH}$ ,  $\text{CH}_3\text{COONa}$ , 0-5  $^\circ\text{C}$ ; **iv.** Hydrazine hydrate,  $\text{EtOH}$ , reflux, 8 h; **v.** Dry xylene, reflux, 6 h; **vi.**  $\text{CH}_3\text{COOH}$ , reflux, 8 h.

The synthesis of pyrazolopyrimidines (**10a-d**) was accomplished via the cyclo-condensation of aminopyrazoles (**6a-d**) with coumarin enaminone (**9**) in glacial acetic acid. The formation of compounds (**10a-d**) is presumed to occur through the nucleophilic attack of the exocyclic amino group in amino pyrazole derivatives (**6a-d**) on the activated double bond in the enaminone (**9**). This results in the generation of acyclic non-isolable intermediates, which subsequently undergo cyclization and aromatization, accompanied by the eliminating of a water molecule, leading to the final isolable products (**10a-d**), as illustrated in **Figure 4**. H. A. Abdel-Aziz et al. demonstrated that this type of reaction occurs through the proposed pathway, as evidenced by the X-ray crystal structure of a similar compound [39].

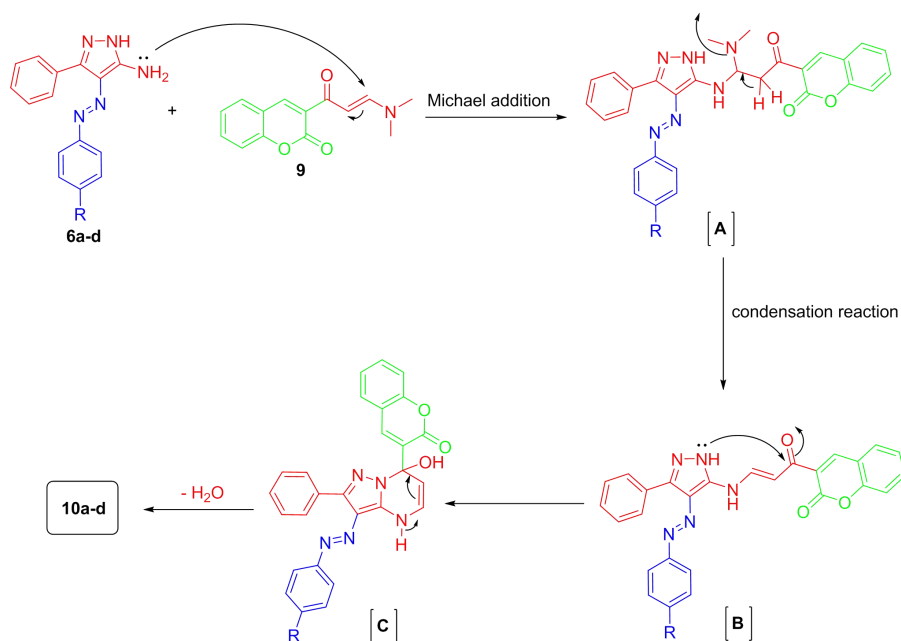


**Figure 4.** Proposed mechanism for the cyclization of **10a-d**.

### 3.2. Biological evaluation

#### 3.2.1. In-vitro anti-cancer activity

The target compounds (**10a-d**) were evaluated for their anti-proliferative activity at a concentration of 10  $\mu$ M in the National Cancer Institute (NCI, Bethesda, Maryland, USA) against a panel of 59 cancer cell lines derived from nine distinct cancer types [32]. To achieve optimal anti-proliferative effects of our compounds, we initially conceptualized the standard diazophenyl ring at the forefront of our designed compounds, as illustrated in compound (**10a**), which did not demonstrate any significant effect. Our study aimed to investigate the lipophilicity and electronegativity characteristics of three substituents: methyl, fluoride, and chloride atoms. The lipophilic nature of the chloride substitution, as observed in compound (**10d**), demonstrated the lowest efficacy among the three substitutions, yielding a mean growth inhibition percentage (GI %) of 27%. In contrast, the reduction of lipophilicity from chloride to a methyl group, as seen in compound (**10b**), resulted in an improved mean GI %, which was 36%. Subsequently, we introduced the fluorine atom at the para position to examine its effects, given that fluorine's low lipophilicity and high electronegativity contribute to a polar character, thereby improving the hydrogen bond acceptor capacity, as demonstrated in compound (**10b**). Compound (**10b**) demonstrated the most favorable outcomes, exhibiting a mean GI % of 50%, indicating that the fluoride atom is optimal for the design, as illustrated in **Table 1**.

**Table 1.** Percentage growth inhibition (GI%) of *in-vitro* subpanel tumor cell lines treated with target coumarins **10a-d** at a concentration of 10  $\mu$ M.

Subpanel	Compounds <sup>a</sup>			
	10a	10b	10c	10d
<b>Leukemia</b>				
CCRF-CEM	-	19	42	33
HL-60(TB)	-	36	-	-
K-562	18	60	54	21
MOLT-4	-	13	29	-
RPMI-8226	-	22	46	22
SR	-	56	53	39
<b>Non-Small Cell Lung Cancer</b>				
A549/ATCC	-	27	83	44
EKVX	-	-	28	24
HOP-62	50	78	83	60
HOP-92	19	53	71	41
NCI-H226	33	94	70	47
NCI-H23	-	15	44	24
NCI-H322M	-	22	36	24
NCI-H460	-	57	97	64
NCI-H522	-	20	47	26
<b>Colon Cancer</b>				
COLO 205	-	-	63	-
HCC-2998	-	22	11	-

HCT-116	12	38	75	40
HCT-15	-	20	34	14
HT29	-	39	49	13
KM12	-	15	48	25
SW-620	-	17	63	36
<b>CNS Cancer</b>				
SF-268	21	33	32	32
SF-295	-	25	27	22
SF-539	16	82	90	51
SNB-19	20	45	63	35
SNB-75	-	30	16	12
U251	11	56	87	66
<b>Melanoma</b>				
LOX IMVI	13	37	78	37
MALME-3M	-	33	37	33
M14	-	31	35	27
MDA-MB435	-	43	45	31
SK-MEL-28	-	51	47	37
SK-MEL-5	30	27	49	44
UACC-257	-	15	30	-
UACC-62	17	36	49	43
<b>Ovarian Cancer</b>				
IGROV1	-	-	16	-
OVCAR-3	-	33	96	40
OVCAR-4	11	49	75	54
OVCAR-5	-	21	33	14
OVCAR-8	22	42	65	32
NCI/ADRRES	-	32	52	25
SK-OV-3	-	16	30	15
<b>Renal Cancer</b>				
786-0	-	55	44	-
A498	-	-	18	-
ACHN	11	63	41	19
CAKI-1	16	74	69	14
RXF 393	15	76	82	32
SN12C	-	30	56	28
TK-10	-	21	39	20
UO-31	-	23	21	-
<b>Prostate Cancer</b>				
PC-3	12	39	44	19
DU-145	-	25	51	50
<b>Breast Cancer</b>				
MCF7	16	22	35	25
MDA-MB231	13	37	49	24
HS 578T	23	60	67	24
BT-549	-	11	-	30
T-47D	16	44	66	50
MDA-MB468	16	38	104	45
<b>Mean inhibition %</b>	-	36	50	27
<b>Sensitive celllines no.</b>	23	55	57	50
<b>Range</b>	11 - 50	11 - 94	11 - 104	12 - 66

<sup>a</sup> Compounds inhibiting growth by more than 10% throughout the NCI-59 cell line panel are only displayed.

In evaluating the efficacy of the novel derivatives (**10a-d**) against nine distinct cancers, the findings are as follows: For leukemia, compound **10a** exhibited negligible activity, while **10b** demonstrated robust activity, achieving the highest inhibition rates of 60% for K-562 and 56% for SR. Compound **10c** displayed moderate to good activity, particularly with inhibition rates of 54% for K-562 and 53% for SR. Lastly, **10d** revealed moderate activity, with SR at 39% and CCRF-CEM at 33%. In the context of NSCLC, compound **10a** exhibited weak activity, with HOP-62 demonstrating the highest inhibition at 50%. Compound **10b** displayed good activity, notably inhibiting NCI-H226 at 94% and HOP-62 at 78%. Compound **10c** revealed exceptional activity, with NCI-H460 (97%), A549/ATCC (83%), and HOP-92 (83%) as the most effectively targeted cell lines. Compound **10d** indicated moderate activity, with NCI-H460 at 64% and HOP-62 at 60%, yielding promising results. Compound **10a** showed minimal activity in all subtypes of colon cancer. Compound **10b** had moderate activity, demonstrating the greatest inhibition of 39% against HT29 cells. **10c** showed significant action, especially in HCT-116 (75%), COLO 205 (63%), and SW-620 (63%). Compound **10d** exhibited weak to moderate activity, with HCT-116 demonstrating the highest efficacy at 40%. In CNS cancer, **10a** had little activity, with the optimal outcome being 21% for SF-268. Compound **10b**

exhibited moderate inhibition of SF-539 (82%) and SNB-19 (45%). Compound **10c** showed moderate to good efficacy, especially for SF-539 (90%). **10d** had minimal activity, with the most significant inhibition observed for U251 (66%). Compound **10a** exhibited minimal inhibitory activity against most cell line panels, except for SK-MEL-5 (30%), in the context of melanoma. In contrast, compounds **10b** and **10c** exhibited moderate to excellent activity on SK-MEL-28 (51%) and LOX IMVI (78%), respectively. Ultimately, compound **10d** exhibited low to moderate activity on the cell panels, with SK-MEL-5 exhibiting the most favorable results at 44%. The OVCAR-4 ovarian cancer cell line panel exhibited a diverse array of activities contingent upon the compound tested. Compounds **10a-d** exhibited inhibitory percentages ranging from 11% to 75%. Compound **10c** exhibited the most favorable results among the four derivatives, exhibiting a 96% inhibitory value towards OVCAR-3. In renal cancer, the cell line panel that exhibited the most significant response to the designed compounds was RXF 393. Compounds **10a-d** exhibited 15%, 76%, 82%, and 32%, respectively. The average mean calculated for the two prostate cancer cell panels PC-3 and DU-145 ranged from 6 to 48%, highlighting compound **10c** as the most potent derivative for this type of cancer. Compound **10c** had the best result across all six cell line panels for breast cancer, with a mean efficacy of 54%. With a growth inhibitory percentage of 104%, MDA-MB468 was the cell line most impacted by compound **10c**.

**Figure 5** shows the results of a heat map analysis applied to the average values of the cell line subpanels within each of the nine cancer types. Compound **10c** stood out among the four derivatives because of its impressive efficacy against four different forms of cancer—NSCL, CNS, ovarian, and breast—with an average success rate of over 50%. Because of this result, the compound is now considered a promising first step in searching for new anti-cancer drugs.

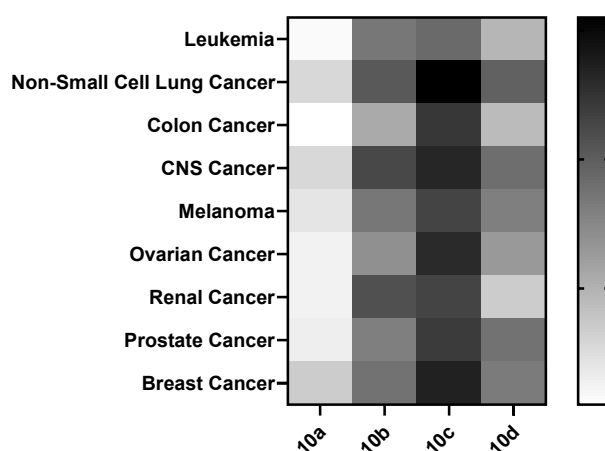


**Figure 5.** Heatmap representation of the *in-vitro* anti-cancer activity of synthesized derivatives (**10a-d**) across nine different cancer subpanels. The intensity of the color indicates the percentage of growth inhibition, highlighting the varying effectiveness of the compounds against distinct cancer cell lines.

### 3.3. In-silico investigation

#### 3.3.1. Kinase profiling

Kinases are essential in cellular signaling, governing processes including growth, differentiation, apoptosis, and metabolism, thus serving as important targets in cancer therapy. AAK1 (Adaptor-associated kinase 1) regulates endocytic trafficking and impacts cancer cell invasion and metastasis [40]. ABL1 (Abelson tyrosine kinase) is implicated in oncogenic transformations and serves as a critical target in chronic myeloid leukemia (CML) [41]. ALK (Anaplastic lymphoma kinase) is commonly mutated in lung cancers, facilitating tumor proliferation [42]. AurA (Aurora kinase A) is crucial for assembling the mitotic spindle, and its dysregulation contributes to tumor chromosomal instability [43]. BRAF, a serine/threonine kinase, is frequently mutated in melanoma and various other cancers, activating the MAPK pathway [44]. Bruton's tyrosine kinase (BTK) is essential in B-cell malignancies, positioning it as a significant target for hematological cancers [45]. CDK2 (Cyclin-dependent kinase 2) plays a critical role in regulating cell cycle progression, and its inhibition presents a viable strategy for impeding tumor growth [46]. CHK1 (Checkpoint kinase 1) plays a pivotal role in mediating DNA damage responses, essential for preserving genomic stability in cancer cells [47]. DYRK1A (Dual-specificity tyrosine-phosphorylation-regulated kinase 1A) plays a role in neuronal development and is also implicated in cell proliferation and survival in specific cancers [48]. EGFR (Epidermal Growth Factor Receptor) is frequently overexpressed or mutated in various cancers, such as lung and breast cancer, contributing to aggressive tumor growth [49]. FAK1 (Focal adhesion kinase 1) facilitates cancer cell adhesion, migration, and invasion, which are essential processes for metastasis [50]. FGFR1 (Fibroblast growth factor receptor 1) promotes angiogenesis and tumor progression, particularly in breast and lung cancers [51]. GSK3B (Glycogen synthase kinase 3 beta) plays a significant role in multiple oncogenic pathways and is associated with the survival of tumor cells [52]. JAK1 (Janus kinase 1) plays a role in cytokine signaling, and its dysregulation is associated with hematological malignancies [53]. MAPK10 (Mitogen-activated protein kinase 10) plays a significant role in apoptosis and stress response, exhibiting both promoting and inhibiting effects on cancer progression [54]. Mutations in PIK3CA (Phosphatidylinositol-4,5-bisphosphate 3-kinase catalytic subunit alpha) result in the activation of the PI3K/AKT/mTOR pathway, which promotes tumorigenesis [55]. PIM1 (Proviral integration site for Moloney murine leukemia virus 1 kinase) promotes survival signaling and confers resistance to apoptosis in cancer cells [56]. VEGFR2 (Vascular Endothelial Growth Factor Receptor 2) plays a crucial role in

angiogenesis, facilitating tumor vascularization and growth [57, 58]. Targeting these kinases provides a comprehensive strategy for disrupting essential oncogenic pathways, thereby playing a crucial role in the advancement of cancer therapeutics.

We conducted *in-silico* kinase profiling to investigate the potential mechanism of action of the potent anti-proliferative compound **10c**. Identifying the molecular targets of the compound was essential for understanding its anti-cancer effects, given its strong activity against the NCI-59 cell line panel. The research focused on molecular docking with a selection of 18 kinases identified for their established involvement in cancer progression and therapeutic significance [59]. This computational method enabled a comparison of the binding affinities of **10c** with co-crystallized ligands for each kinase expressed in kcal/mol.

The docking studies identified two potential kinase targets, JAK1 and CDK2, exhibiting significantly higher binding affinities for **10c** than the respective native ligands, as illustrated in **Table 2** and **Figure 6**. JAK1 and CDK2 are essential kinases in cancer biology; JAK1 participates in cytokine signaling pathways and cell proliferation [60], whereas CDK2 is crucial for regulating the cell cycle [46]. The binding affinities of **10c** to these targets were superior to those of their co-crystallized ligands, indicating a strong potential for interaction and inhibition.

This preliminary screening provides valuable insights into the potential mechanism of action of compound **10c**, highlighting its ability to inhibit key kinases involved in tumor growth and survival. Such findings emphasize the compound's therapeutic potential and warrant further experimental validation to confirm its inhibitory effects on JAK1 and CDK2 and its broader anti-cancer activity.

**Table 2.** The screening was conducted on 18 distinct kinases, providing their PDB codes, release dates, resolution, gene names, full names, and the binding affinities expressed in kcal/mol for both the co-crystallized ligand and our potent compound **10c**.

#	PDB Code	Release Time	Resolution	Gene Name	Full Name	Binding affinity (kcal/mol)	
						Co-crystallized	10c
1	5TE0	2016	1.90	AAK1	AP2-associated protein kinase 1 AAK1	-9.1	-9.6
2	2G2H	2006	2.00	ABL1	Tyrosine-protein kinase ABL1	-11.3	-9.9
3	4Z55	2015	1.55	ALK	ALK tyrosine kinase receptor	-9.2	-10.0
4	5ORL	2017	1.69	AurA	Aurora A kinase AurA	-5.3	-7.3
5	5VAM	2017	2.10	BRAF	Serine/threonine-protein kinase BRAF	-13.6	-11.2
6	3GEN	2010	1.60	BTK	Tyrosine-protein kinase BTK	-10.9	-10.4
7	6Q4G	2019	0.98	CDK2	Cyclin dependent kinase 2 CDK2	-8.0	-10.4
8	4RVM	2014	1.86	CHK1	Serine/threonine-Transferase CHK1	-10.2	-11.6
9	6S1J	2019	1.41	DYRK1A	Dual specificity tyrosine-phosphorylation-regulated kinase 1A DYRK1A	-10.0	-11.3
10	5X2A	2017	1.85	EGFR	Epidermal growth factor receptor	-8.8	-10.2
11	4GU6	2013	1.95	FAK1	Focal adhesion kinase 1 FAK1	-9.6	-9.1
12	5EW8	2016	1.63	FGFR1	Fibroblast growth factor receptor 1 FGFR1	-9.6	-10.5
13	4PTE	2014	2.03	GSK3B	Glycogen synthase kinase-3 beta GSK3B	-8.9	-9.6
14	3EYG	2009	1.90	JAK1	Tyrosine-protein kinase JAK1	-7.9	-10.3
15	4X21	2014	1.95	MAPK10	Mitogen-activated protein kinase 10 MAPK10	-9.0	-10.9
16	4JPS	2014	2.20	PIK3CA	Phosphatidylinositol 4,5-bisphosphate 3-kinase	-9.6	-9.6

					catalytic subunit alpha isoform		
17	5VUC	2017	2.00	PIM1	Serine/threonine-protein kinase PIM1	-10.9	-11.5
18	3WZD	2014	1.57	VEGFR2	Vascular endothelial growth factor receptor 2 VEGFR2	-9.9	-11.2

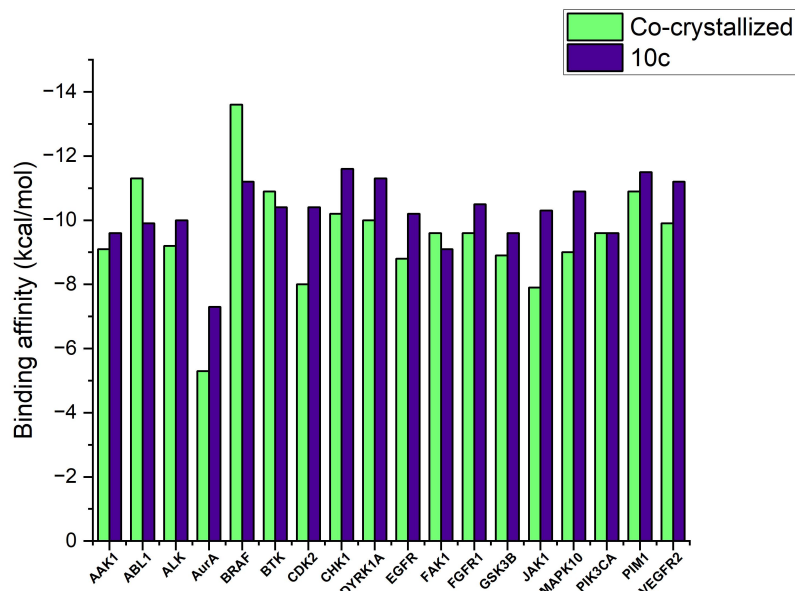


**Figure 6.** The binding affinities for co-crystallized ligands and **10c** on 18 different kinases.

### 3.3.2. Molecular docking studies

Our study involved molecular docking analyses of compound **10c** with JAK1 and CDK2 to elucidate its binding interactions and comprehend the molecular mechanisms contributing to its biological activity. We evaluated the docking poses and binding affinities to identify the key interactions between compound **10c** and the active sites of JAK1 and CDK2, which are critical targets in various signaling pathways and cancer progression [34]. This computational method offered a comprehensive understanding of the molecular recognition and specificity of **10c** while also enabling the optimization of its structural characteristics for improved target engagement. The docking results corroborated our hypothesis that **10c** may exert significant anti-cancer effects by inhibiting both JAK1 and CDK2, providing essential insights for subsequent lead optimization and potential therapeutic applications.

#### 3.3.2.1. Molecular docking analysis of JAK1

Molecular docking studies were performed on the JAK1 enzyme (PDB ID: 3EYG) [36] to investigate the potential binding interactions of our potent molecule **10c**. Validation was conducted before docking studies to confirm the docking protocol, with an RMSD of 1.44 Å between the co-crystallized and redocked molecules, deemed adequate to proceed with the study (Figure 7). The co-crystallized ligand demonstrated a binding affinity of -7.9 kcal/mol, whereas our potent molecule exhibited -10.3 kcal/mol, prompting further investigation into its binding interactions.

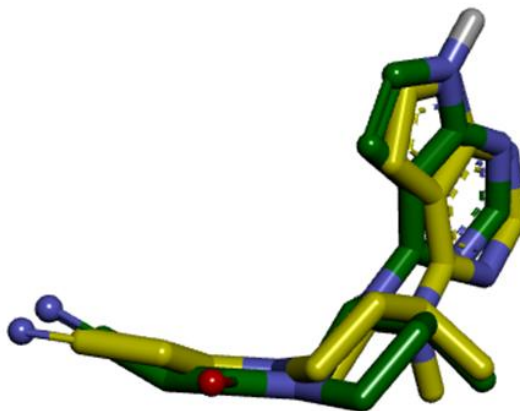


**Figure 7.** Docking validation for JAK1 enzyme was performed using the co-crystallized ligand (yellow) and the redocked one (green).

Compound **10c** preserved the essential hydrogen bonding interaction established by Glu-883 amino acid with the carbonyl group of the coumarin scaffold. A newly formed hydrogen bond was observed between the Asn-1008 amino acid and the pyrazolopyrimidine scaffold. The coumarin scaffold demonstrated its importance in forming two  $\pi$ -anion bonds with Glu-966. The 4-fluorophenyl ring formed  $\pi$ -sulfur interactions with Met-956, while the fluoride atom on the ring engaged in halogen bonding with the Glu-957 amino acid. Hydrophobic interactions were observed in  $\pi$ -alkyl and  $\pi$ - $\sigma$  bonding between the diazophenyl and the attached phenyl ring, as well as the pyrazolopyrimidine scaffold with the amino acids Leu-881, Val-889, Ala-906, Arg-1007, and Leu-1010. (Figure 8)

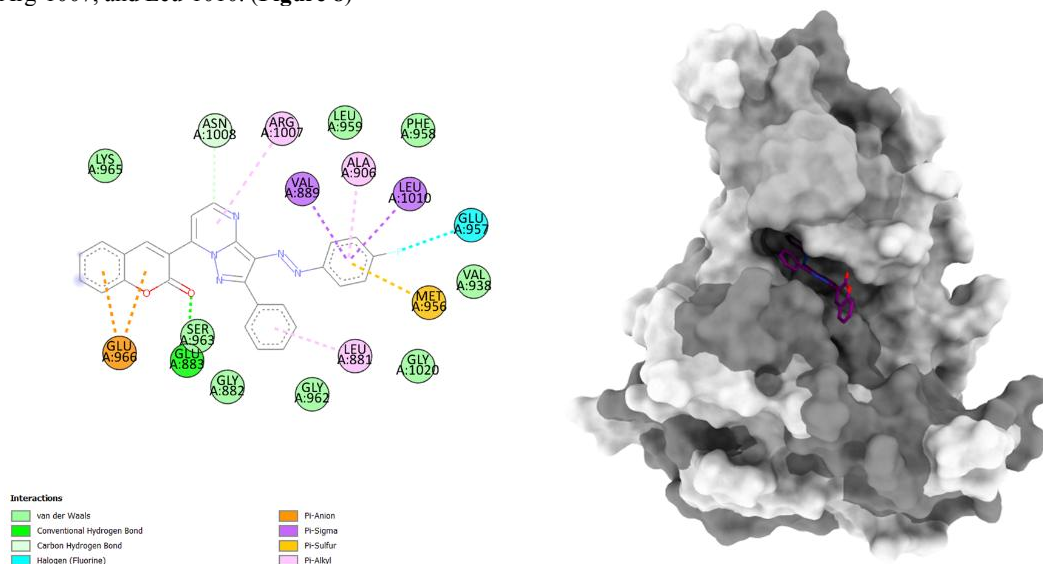


Figure 8. 2D and 3D illustrations of compound **10c** with JAK1.

### 3.3.2.2. Molecular docking on CDK2

In order to explore the possible binding interactions of our potent compound **10c**, molecular docking studies were conducted on the CDK2 enzyme (PDB ID: 6Q4G) [37]. Before conducting docking investigations, validation was carried out to verify the docking methodology. The results showed an acceptable RMSD of 1.08 Å between the co-crystallized and redocked molecules, therefore the study could move forward (Figure 9). We need to investigate further into the binding interactions of our potent molecule because the co-crystallized ligand had a binding affinity of -8.0 kcal/mol and **10c** showed -10.4 kcal/mol.

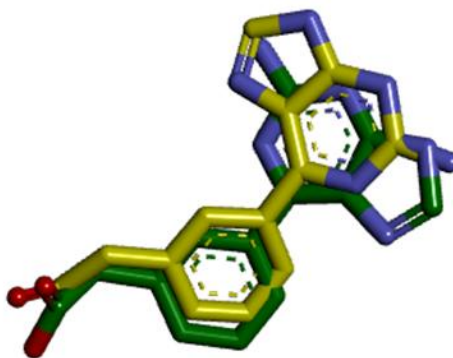
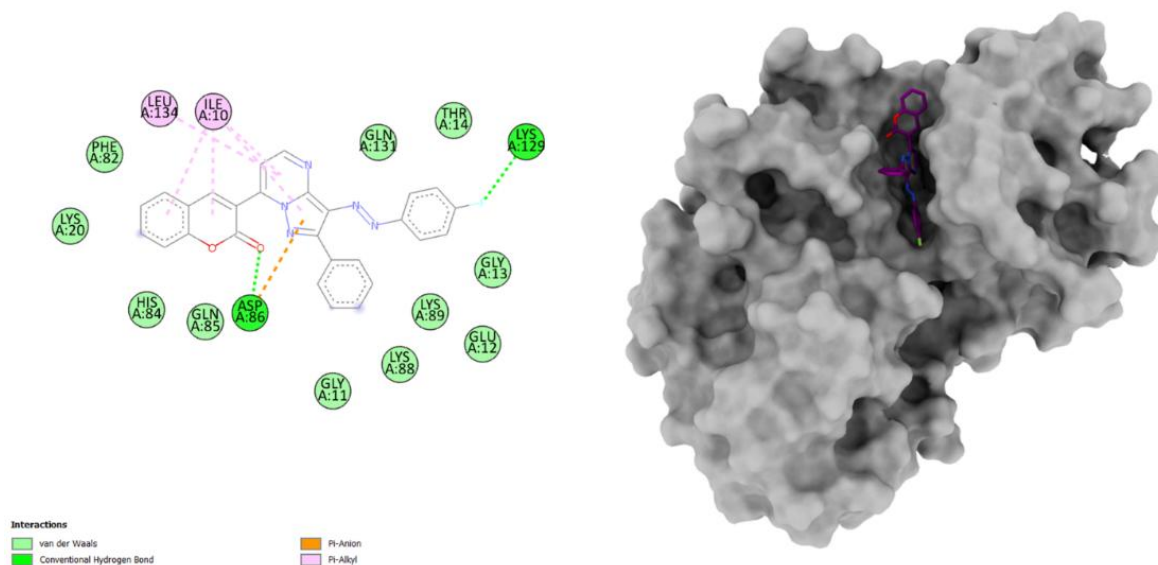


Figure 9. Superimposition of the co-crystallized (yellow) and redocked (green) ligands for the CDK2 enzyme.

Compound **10c** preserved the critical hydrogen bonding interaction with the carbonyl group of the coumarin scaffold, facilitated by the Asp-86 amino acid, alongside a  $\pi$ -anion bond with the pyrazolopyrimidine scaffold. Incorporating a fluorine atom on the diazophenyl ring is significant due to its hydrogen bonding interaction with the Lys-129 amino acid. Hydrophobic interactions were established between the amino acids Ile-10 and Leu-134 with the coumarin and pyrazolopyrimidine linkage. (Figure 10)



**Figure 10.** The binding interactions between compound **10c** and CDK2.

### 3.3.2.3. Analysis of interactions for CAN508 (XVI), XVII, and 10c with JAK1 and CDK2

The docking results for JAK1 indicate unique interaction profiles for the three compounds. **CAN508 (XVI)** establishes a hydrogen bond with Glu-957 through its pyrazole ring and participates in  $\pi$ - $\sigma$  interactions with residues such as Leu-1010, thereby stabilizing the compound within the binding pocket. Compound **XVII**, featuring a pyrazolo[1,5-*a*]pyrimidine linker, establishes a hydrogen bond with Glu-966, whereas its phenyl tail contributes to enhanced hydrophobic interactions. The newly developed **10c** incorporates a coumarin scaffold that engages in hydrogen bonding with Glu-883,  $\pi$ -anion interaction with Glu-966, and halogen bonding through its para-fluorophenyl ring with Glu-957. The distinctive characteristics of **10c** markedly enhance its binding affinity and interaction profile in comparison to **CAN508 (XVI)** and **XVII**. (**Table 3**)

In the case of CDK2, **CAN508 (XVI)** establishes two hydrogen bonds: one with Leu-83 through its hydroxyl group and another with Asp-86 via its pyrazole ring. It participates in hydrophobic interactions with amino acids such as Ile-10 and Leu-134, thereby stabilizing the compound within the binding pocket. Compound **XVII**, featuring a sulfonamide group, establishes supplementary hydrogen bonds with Lys-129 and Thr-165. Additionally, the phenyl ring linked to the pyrazolo[1,5-*a*]pyrimidine moiety amplifies hydrophobic interactions. Conversely, **10c** features a coumarin scaffold that establishes hydrogen bonds with Asp-86, while its para-fluorophenyl ring interacts through hydrogen bonding with Lys-129. The distinctive characteristics of **10c** enhance its binding affinity and interaction profile relative to **CAN508 (XVI)** and **XVII**. (**Figure 11**)

**Table 3.** The binding affinities comparison between the lead molecules (**XVI-XVII**) and our potent compound **10c** on JAK1 and CDK2.

Compounds	Enzyme	Binding affinity (kcal/mol)
<b>CAN508 (XVI)</b>	JAK1	-7.1
<b>XVII</b>	JAK1	-9.6
<b>10c</b>	JAK1	<b>-10.3</b>
<b>CAN508 (XVI)</b>	CDK2	-6.5
<b>XVII</b>	CDK2	-8.6
<b>10c</b>	CDK2	<b>-10.4</b>

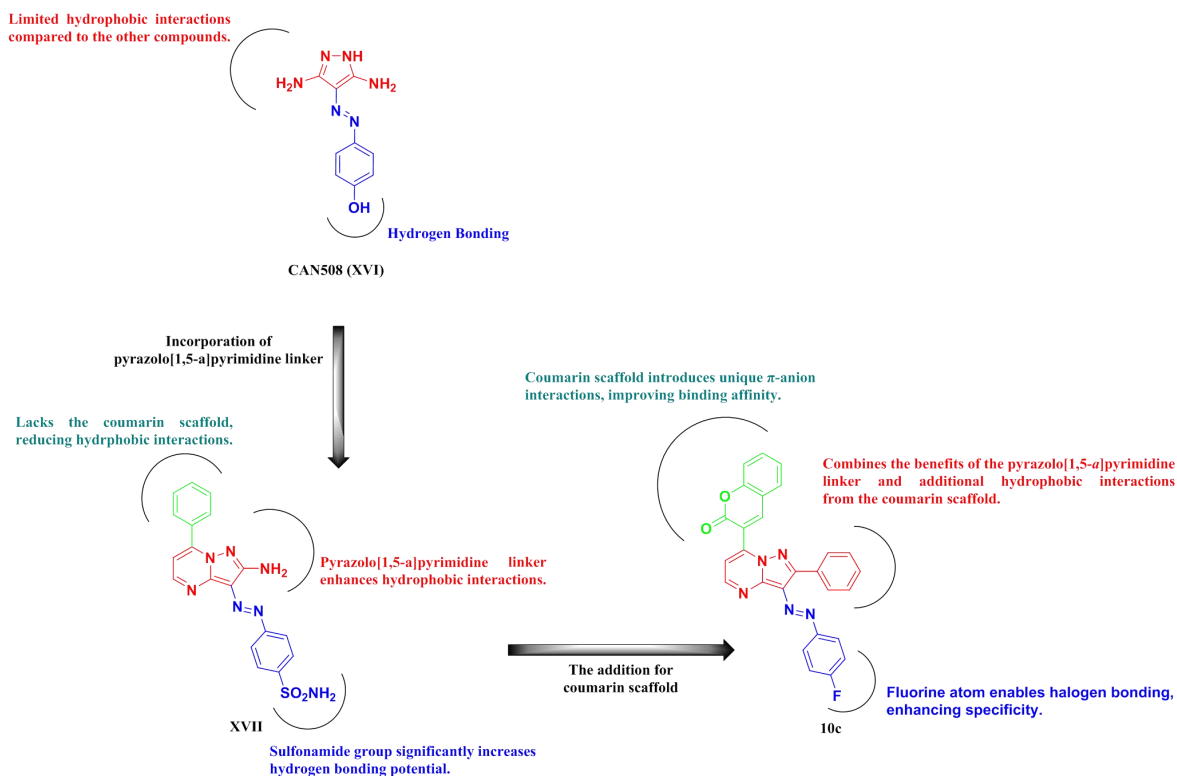


**Figure 11.** Summary of docking interactions for CAN508 (XVI), XVII, and 10c with JAK1 and CDK2.

### 3.3.3. Pharmacokinetic and drug-likeness prediction

ADMETlab 3.0 [33] was utilized to predict the pharmacokinetic properties of compound 10c. **Figure 12** illustrates that compound 10c demonstrated favorable pharmacokinetic characteristics as the compound complies with Lipinski's Rule of Five, suggesting favorable oral bioavailability potential, characterized by a molecular weight (MW) of 461.13, a logP of 4.716, and a topological polar surface area (TPSA) of 85.12 Å<sup>2</sup>, all falling within acceptable limits. The structure exhibits moderate flexibility, characterized by four rotatable bonds (nRot = 4) and a rigidity score (nRig = 35) approaching the optimal range. Furthermore, its physicochemical properties, including the number of hydrogen bond acceptors (nHA = 7) and donors (nHD = 0), align with the optimal range, reinforcing its drug-likeness. However, the maximum values for three attributes—LogP, LogD, and nRig—of compound 10c slightly exceed the 'upper limit' indicated by the blue zone. Other attributes, however, exhibited strong performance. The detailed information from the server can be found in the supplementary material file.

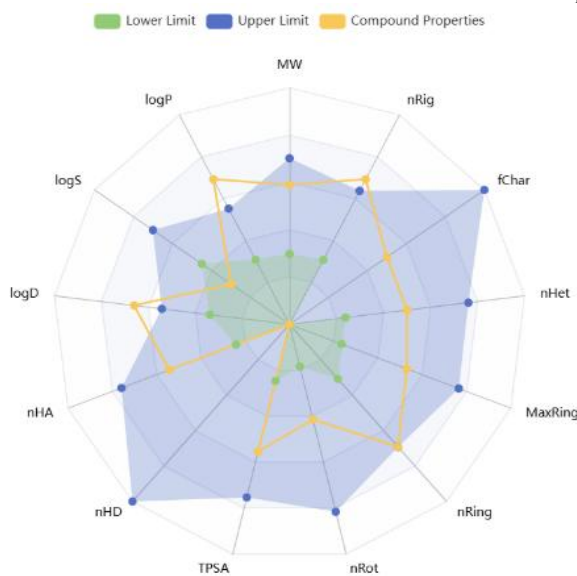


**Figure 12.** Pharmacokinetic mapping for compound 10c derived from ADMETlab 3.0. The upper boundary is delineated by bluish areas, the lower boundary by greenish areas, and the compound parameters are represented by yellowish lines.

### 3.3.4. Evaluation of potential toxicity

To avoid unintended consequences, it is crucial to evaluate the toxicity of compounds. The chemical structures of the molecules were analyzed for potential toxicity risks, including mutagenicity (MUT), tumorigenicity (TUM), irritation (IRRIT), and reproductive effects (RE), using the OSIRIS property explorer [35]. Based on functional group similarities, this tool assesses hazards by comparing the studied molecules to others in its database, which have been previously evaluated *in-vitro* and *in-vivo*. The findings indicate that most tested compounds are relatively safe, exhibiting low to moderate toxicity concerning mutagenicity, irritation, and reproductive effects (Table 4). However, all of the compounds showed harmful effects in terms of tumorigenicity.

The acute toxicity of the targeted coumarin derivatives **10a-d** was predicted in this study using the ProTox-III platform [56]. As shown in Table 4, most of the compounds are anticipated to belong to the slightly hazardous class 4, with LD<sub>50</sub> values falling around the 1000 mg/kg range. This toxicity level is categorized as class 4 out of 6, indicating mild toxicity, particularly when administered orally. Detailed toxicity profiles generated by ProTox-III can be found in the supplementary materials (Table S3). Overall, further research is strongly recommended to optimize and thoroughly investigate the pharmacological potential of these compounds, as they demonstrate significant promise.

**Table 4.** Possible toxicity issues with the particular compounds being studied.

Compound	Chronic Toxicity Risks <sup>a</sup> (OSIRIS)				Acute Oral Toxicity <sup>b</sup> (ProTox-III)	
	MUT	TUM	IRRIT	RE	LD <sub>50</sub> (mg/kg)	Toxicity Class (1-6)
<b>10a</b>					1000	4
<b>10b</b>					1000	4
<b>10c</b>					1000	4
<b>10d</b>					5000	5

<sup>a</sup>The outcomes are categorized into three distinct colors: red, green, and orange. The color green is indicative of a low potential for toxicity. In contrast, orange signifies a mild level of toxicity, and red indicates a high likelihood of toxicity.

<sup>b</sup>The toxicity class on a scale of 1 to 6 represents varying levels of risk. Class 1 is classified as fatal if ingested (LD<sub>50</sub> ≥ 5 mg/kg), class 2 is classified as fatal if ingested (5 ≥ LD<sub>50</sub> ≥ 50 mg/kg), class 3 is classified as toxic if ingested (50 ≥ LD<sub>50</sub> ≥ 300 mg/kg), class 4 is classified as harmful if ingested (300 ≥ LD<sub>50</sub> ≥ 2000 mg/kg), class 5 is classified as potentially harmful if ingested (2000 ≥ LD<sub>50</sub> ≥ 5000 mg/kg), and class 6 is classified as nontoxic (LD<sub>50</sub> > 5000 mg/kg).

## 4. Conclusion

We synthesized a series of novel pyrazolopyrimidine-coumarin derivatives (**10a-d**) as potential anti-cancer agents. We assessed their biological activity against the NCI-59 cell line panel, which includes nine distinct cancer types. Among the synthesized derivatives, compound **10c** was identified as the most promising candidate, exhibiting a mean growth inhibition of 50% across all 59 cell lines. We conducted *in-silico* molecular docking studies on 18 kinases to elucidate the potential mechanism of action, identifying JAK1 and CDK2 as key targets with favorable binding affinities similar to co-crystallized ligands. Further analysis indicated that compound **10c** maintained crucial hydrogen bonding interactions with Glu-883 and Asp-86 on JAK1 and CDK2, respectively, facilitated by the coumarin scaffold's carbonyl moiety, underscoring this structural feature's importance in its design. Pharmacokinetic, drug-likeness, and toxicity predictions performed with ADMETLab 3.0, OSIRIS Property Explorer, and ProTox-III webserver indicated the drug-like potential of compound **10c**, reinforcing its suitability as a lead molecule for further development. The findings highlight the therapeutic potential of compound **10c** as an anti-cancer agent and facilitate the design and synthesis of new derivatives targeting JAK1 and CDK2 to mitigate resistance and toxicity linked to current treatments. Subsequent research will refine these scaffolds to improve their efficacy and selectivity.

### CRedit authorship contribution statement

**Mahmoud S. Elkotamy:** Writing – original draft, Investigation, Data curation, Software. **Mohamed A. Abdelrahman:** Writing – review & editing, Supervision. **Wagdy M. Eldehna:** Validation, Supervision, Methodology, Formal analysis, Conceptualization. **Hatem A. Abdel-Aziz:** Project administration, Supervision, Validation, Methodology, Formal analysis, Conceptualization. **Sahar M. Abou-Seri:** Writing – review & editing, Writing – original draft, Validation, Supervision, Methodology, Data curation, Conceptualization.

### Declaration of competing interest

The authors declare that they have no known competing financial interests or personal relationships that could have appeared to influence the work reported in this paper.

## 5. References

- [1] H. Sung, J. Ferlay, R.L. Siegel, M. Laversanne, I. Soerjomataram, A. Jemal, F. Bray, Global cancer statistics 2020: GLOBOCAN estimates of incidence and mortality worldwide for 36 cancers in 185 countries, *CA: a cancer journal for clinicians* 71(3) (2021) 209-249.
- [2] K. Bukowski, M. Kciuk, R. Kontek, Mechanisms of multidrug resistance in cancer chemotherapy, *International journal of molecular sciences* 21(9) (2020) 3233.
- [3] X.-x. Sun, Q. Yu, Intra-tumor heterogeneity of cancer cells and its implications for cancer treatment, *Acta Pharmacologica Sinica* 36(10) (2015) 1219-1227.
- [4] X. Jiang, J. Wang, X. Deng, F. Xiong, S. Zhang, Z. Gong, X. Li, K. Cao, H. Deng, Y. He, The role of microenvironment in tumor angiogenesis, *Journal of Experimental & Clinical Cancer Research* 39 (2020) 1-19.
- [5] M.A. Feitelson, A. Arzumanyan, R.J. Kulathinal, S.W. Blain, R.F. Holcombe, J. Mahajna, M. Marino, M.L. Martinez-Chantar, R. Nawroth, I. Sanchez-Garcia, Sustained proliferation in cancer: Mechanisms and novel therapeutic targets, *Seminars in cancer biology*, Elsevier, 2015, pp. S25-S54.
- [6] R.B. Mokhtari, T.S. Homayouni, N. Baluch, E. Morgatskaya, S. Kumar, B. Das, H. Yeger, Combination therapy in combating cancer, *Oncotarget* 8(23) (2017) 38022.
- [7] J. Hoult, M. Payá, Pharmacological and biochemical actions of simple coumarins: natural products with therapeutic potential, *General Pharmacology: The Vascular System* 27(4) (1996) 713-722.
- [8] M.A. Abdelrahman, H.S. Ibrahim, A. Nocentini, W.M. Eldehna, A. Bonardi, H.A. Abdel-Aziz, P. Gratteri, S.M. Abou-Seri, C.T. Supuran, Novel 3-substituted coumarins as selective human carbonic anhydrase IX and XII inhibitors: Synthesis, biological and molecular dynamics analysis, *European Journal of Medicinal Chemistry* 209 (2021) 112897.
- [9] H.S. Ibrahim, M.A. Abdelrahman, A. Nocentini, S. Bua, H.A. Abdel-Aziz, C.T. Supuran, S.M. Abou-Seri, W.M. Eldehna, Insights into the effect of elaborating coumarin-based aryl enamines with sulfonamide or carboxylic acid functionality on carbonic anhydrase inhibitory potency and selectivity, *Bioorganic Chemistry* 126 (2022) 105888.
- [10] A.K. El-Damasy, H.J. Kim, A. Nocentini, S.H. Seo, W.M. Eldehna, E.-K. Bang, C.T. Supuran, G. Keum, Discovery of new 6-ureido/amidocoumarins as highly potent and selective inhibitors for the tumour-relevant carbonic anhydrases IX and XII, *Journal of Enzyme Inhibition and Medicinal Chemistry* 38(1) (2023) 2154603.
- [11] K.M. Amin, A.M. Taha, R.F. George, N.M. Mohamed, F.F. Elsenduny, Synthesis, antitumor activity evaluation, and DNA-binding study of coumarin-based agents, *Archiv Der Pharmazie* 351(1) (2018) 1700199.
- [12] I. Hueso-Falcon, A. Amesty, L. Anaissi-Afonso, I. Lorenzo-Castrillejo, F. Machin, A. Estevez-Braun, Synthesis and biological evaluation of naphthoquinone-coumarin conjugates as topoisomerase II inhibitors, *Bioorganic & medicinal chemistry letters* 27(3) (2017) 484-489.
- [13] E.R. El-Sawy, M.S. Ebaid, H.M. Rady, A.B. Shalby, K.M. Ahmed, H.M. Abo-Salem, Synthesis and molecular docking of novel non-cytotoxic anti-angiogenic sulfonyl coumarin derivatives against hepatocellular carcinoma cells in vitro, *Journal of Applied Pharmaceutical Science* 7(2) (2017) 049-066.
- [14] G.S. Lingaraju, K.S. Balaji, S. Jayarama, S.M. Anil, K.R. Kiran, M.P. Sadashiva, Synthesis of new coumarin tethered isoxazolines as potential anticancer agents, *Bioorganic & medicinal chemistry letters* 28(23-24) (2018) 3606-3612.
- [15] S.L. Park, S.Y. Won, J.-H. Song, S.-Y. Lee, W.-J. Kim, S.-K. Moon, Esculetin inhibits VEGF-induced angiogenesis both in vitro and in vivo, *The American Journal of Chinese Medicine* 44(01) (2016) 61-76.
- [16] D. Cao, Y. Liu, W. Yan, C. Wang, P. Bai, T. Wang, M. Tang, X. Wang, Z. Yang, B. Ma, Design, synthesis, and evaluation of in vitro and in vivo anticancer activity of 4-substituted coumarins: a novel class of potent tubulin polymerization inhibitors, *Journal of medicinal chemistry* 59(12) (2016) 5721-5739.
- [17] H. Singh, J.V. Singh, M.K. Gupta, A.K. Saxena, S. Sharma, K. Nepali, P.M.S. Bedi, Triazole tethered isatin-coumarin based molecular hybrids as novel antitubulin agents: Design, synthesis, biological investigation and docking studies, *Bioorganic & medicinal chemistry letters* 27(17) (2017) 3974-3979.
- [18] R.M. Abdelnaby, H.S. Rateb, O. Ali, A.S. Saad, R.I. Nadeem, S.M. Abou-Seri, K.M. Amin, N.S. Younis, R. Abdelhady, Dual PI3K/Akt inhibitors bearing coumarin-thiazolidine pharmacophores as potential apoptosis inducers in MCF-7 cells, *Pharmaceuticals* 15(4) (2022) 428.
- [19] H.I. Abdelaal, A.R. Mohamed, M.F. Abo-Ashour, S. Giovannuzzi, S.H. Fahim, H.A. Abdel-Aziz, C.T. Supuran, S.M. Abou-Seri, Mitigating the resistance of MCF-7 cancer cells to Doxorubicin under hypoxic conditions with novel coumarin based carbonic anhydrase IX and XII inhibitors, *Bioorganic Chemistry* 152 (2024) 107759.
- [20] W.B. Parker, Enzymology of purine and pyrimidine antimetabolites used in the treatment of cancer, *Chemical reviews* 109(7) (2009) 2880-2893.
- [21] R.A. Mesa, U. Yasothan, P. Kirkpatrick, Ruxolitinib, *Nature reviews Drug discovery* 11(2) (2012) 103-105.
- [22] S. Dhillon, Tofacitinib: a review in rheumatoid arthritis, *Drugs* 77 (2017) 1987-2001.
- [23] A. Markham, Baricitinib: first global approval, *Drugs* 77(6) (2017) 697-704.
- [24] M. Talpaz, J.-J. Kiladjian, Fedratinib, a newly approved treatment for patients with myeloproliferative neoplasm-associated myelofibrosis, *Leukemia* 35(1) (2021) 1-17.
- [25] K.R. Abdellatif, R.B. Bakr, Pyrimidine and fused pyrimidine derivatives as promising protein kinase inhibitors for cancer treatment, *Medicinal Chemistry Research* 30 (2021) 31-49.
- [26] A.C. Borisa, H.G. Bhatt, A comprehensive review on Aurora kinase: Small molecule inhibitors and clinical trial studies, *European journal of medicinal chemistry* 140 (2017) 1-19.
- [27] P.K. Maji, Recent progress in the synthesis of pyrimidine heterocycles: A review, *Current Organic Chemistry* 24(10) (2020) 1055-1096.

- [28] V. Kryštof, L. Rárová, J. Liebl, S. Zahler, R. Jorda, J. Voller, P. Cankař, The selective P-TEFb inhibitor CAN508 targets angiogenesis, *European journal of medicinal chemistry* 46(9) (2011) 4289-4294.
- [29] M.A. Said, W.M. Eldehna, A. Nocentini, S.H. Fahim, A. Bonardi, A.A. Elgazar, V. Kryštof, D.H. Soliman, H.A. Abdel-Aziz, P. Gratteri, S.M. Abou-Seri, C.T. Supuran, Sulfonamide-based ring-fused analogues for CAN508 as novel carbonic anhydrase inhibitors endowed with antitumor activity: Design, synthesis, and in vitro biological evaluation, *European Journal of Medicinal Chemistry* 189 (2020) 112019.
- [30] I.S. Hafiz,  $\beta$ -Enaminonitriles in Heterocyclic Synthesis: Synthesis of New 1, 4-Dihydropyridine, Pyrazolo [1, 5-a] pyrimidine, Aminothiophene and Pyridine Derivatives, *Zeitschrift für Naturforschung B* 55(3-4) (2000) 321-325.
- [31] F.M.A.A. El-Taweel, M.H. Elnagdi, Studies with enamines: synthesis of new coumarin-3-yl azoles, coumarin-3-yl azines, coumarin-3-yl azoloazines, coumarin-3-yl pyrone and coumarin-2-yl benzo [b] furans, *Journal of Heterocyclic Chemistry* 38(4) (2001) 981-984.
- [32] M.R. Grever, S.A. Schepartz, B.A. Chabner, The National Cancer Institute: cancer drug discovery and development program, *Seminars in oncology*, 1992, pp. 622-638.
- [33] L. Fu, S. Shi, J. Yi, N. Wang, Y. He, Z. Wu, J. Peng, Y. Deng, W. Wang, C. Wu, ADMETlab 3.0: an updated comprehensive online ADMET prediction platform enhanced with broader coverage, improved performance, API functionality and decision support, *Nucleic Acids Research* (2024) gkae236.
- [34] M.S. Elkotamy, M.K. Elgohary, I.A. Elkelesh, A.M. Hamdy, Discovering new CDK2 inhibitors by molecular docking and drug-likeness-based virtual screening for potential anticancer uses, *ERU Research Journal* (2024).
- [35] M.S. Elkotamy, M.K. Elgohary, S.T. Al-Rashood, H. Almahli, W.M. Eldehna, H.A. Abdel-Aziz, Novel imidazo [2, 1-b] thiazoles and imidazo [1, 2-a] pyridines tethered with indolinone motif as VEGFR-2 inhibitors and apoptotic inducers: Design, synthesis and biological evaluations, *Bioorganic Chemistry* 151 (2024) 107644.
- [36] N.K. Williams, R.S. Bamert, O. Patel, C. Wang, P.M. Walden, A.F. Wilks, E. Fantino, J. Rossjohn, I.S. Lucet, Dissecting specificity in the Janus kinases: the structures of JAK-specific inhibitors complexed to the JAK1 and JAK2 protein tyrosine kinase domains, *Journal of molecular biology* 387(1) (2009) 219-232.
- [37] D.J. Wood, J.D. Lopez-Fernandez, L.E. Knight, I. Al-Khawaldeh, C. Gai, S. Lin, M.P. Martin, D.C. Miller, C. Cano, J.A. Endicott, FragLites—minimal, halogenated fragments displaying pharmacophore doublets. An efficient approach to druggability assessment and hit generation, *Journal of Medicinal Chemistry* 62(7) (2019) 3741-3752.
- [38] P.K. Sharma, K. Singh, S. Kumar, P. Kumar, S. Dhawan, S. Lal, H. Ulbrich, G. Dannhardt, Synthesis and anti-inflammatory evaluation of some pyrazolo [3, 4-b] pyridines, *Medicinal chemistry research* 20 (2011) 239-244.
- [39] H.A. Abdel-Aziz, T.S. Saleh, H.S. El-Zahabi, Facile synthesis and in-vitro antitumor activity of some pyrazolo [3, 4-b] pyridines and pyrazolo [1, 5-a] pyrimidines linked to a thiazolo [3, 2-a] benzimidazole moiety, *Archiv der Pharmazie: An International Journal Pharmaceutical and Medicinal Chemistry* 343(1) (2010) 24-30.
- [40] S.D. Conner, S.L. Schmid, Identification of an adaptor-associated kinase, AAK1, as a regulator of clathrin-mediated endocytosis, *The Journal of cell biology* 156(5) (2002) 921-929.
- [41] E. De Braekeleer, N. Douet-Guilbert, D. Rowe, N. Bown, F. Morel, C. Berthou, C. Férec, M. De Braekeleer, ABL1 fusion genes in hematological malignancies: a review, *European journal of haematology* 86(5) (2011) 361-371.
- [42] B. Hallberg, R. Palmer, The role of the ALK receptor in cancer biology, *Annals of Oncology* 27 (2016) iii4-iii15.
- [43] V.M. Bolanos-Garcia, Aurora kinases, *The international journal of biochemistry & cell biology* 37(8) (2005) 1572-1577.
- [44] H. Davies, G.R. Bignell, C. Cox, P. Stephens, S. Edkins, S. Clegg, J. Teague, H. Woffendin, M.J. Garnett, W. Bottomley, Mutations of the BRAF gene in human cancer, *Nature* 417(6892) (2002) 949-954.
- [45] J.J. Buggy, L. Elias, Bruton tyrosine kinase (BTK) and its role in B-cell malignancy, *International reviews of immunology* 31(2) (2012) 119-132.
- [46] S. Tadesse, A.T. Anshabo, N. Portman, E. Lim, W. Tilley, C.E. Caldon, S. Wang, Targeting CDK2 in cancer: challenges and opportunities for therapy, *Drug discovery today* 25(2) (2020) 406-413.
- [47] Y. Zhang, T. Hunter, Roles of Chk1 in cell biology and cancer therapy, *International journal of cancer* 134(5) (2014) 1013-1023.
- [48] J. Wegiel, C.X. Gong, Y.W. Hwang, The role of DYRK1A in neurodegenerative diseases, *The FEBS journal* 278(2) (2011) 236-245.
- [49] R.I. Nicholson, J.M.W. Gee, M.E. Harper, EGFR and cancer prognosis, *European journal of cancer* 37 (2001) 9-15.
- [50] E.-Z. Dayang, M. Luxen, T. Kuiper, R. Yan, S. Rangarajan, M. van Meurs, J. Moser, G. Molema, Pharmacological inhibition of focal adhesion kinase 1 (FAK1) and anaplastic lymphoma kinase (ALK) identified via kinome profile analysis attenuates lipopolysaccharide-induced endothelial inflammatory activation, *Biomedicine & Pharmacotherapy* 133 (2021) 111073.
- [51] J. Weiss, M.L. Sos, D. Seidel, M. Peifer, T. Zander, J.M. Heuckmann, R.T. Ullrich, R. Menon, S. Maier, A. Soltermann, Frequent and focal FGFR1 amplification associates with therapeutically tractable FGFR1 dependency in squamous cell lung cancer, *Science translational medicine* 2(62) (2010) 62ra93-62ra93.
- [52] W.F. An, A.R. Germain, J.A. Bishop, P.P. Nag, S. Metkar, J. Ketterman, M. Walk, M. Weiwer, X. Liu, D. Patnaik, Discovery of potent and highly selective inhibitors of GSK3 $\beta$ , *Probe Reports from the NIH Molecular Libraries Program [Internet]* (2014).
- [53] H. Xiong, Z.-G. Zhang, X.-Q. Tian, D.-F. Sun, Q.-C. Liang, Y.-J. Zhang, R. Lu, Y.-X. Chen, J.-Y. Fang, Inhibition of JAK1, 2/STAT3 signaling induces apoptosis, cell cycle arrest, and reduces tumor cell invasion in colorectal cancer cells, *Neoplasia* 10(3) (2008) 287-297.

- [54] J. Ying, H. Li, Y. Cui, A. Wong, C. Langford, Q. Tao, Epigenetic disruption of two proapoptotic genes MAPK10/JNK3 and PTPN13/FAP-1 in multiple lymphomas and carcinomas through hypermethylation of a common bidirectional promoter, *Leukemia* 20(6) (2006) 1173-1175.
- [55] R. Arafeh, Y. Samuels, PIK3CA in cancer: The past 30 years, *Seminars in cancer biology*, Elsevier, 2019, pp. 36-49.
- [56] F.A. Binjubair, B.S. Almansour, N.I. Ziedan, A.A.M. Abdel-Aziz, S.T. Al-Rashood, M.K. Elgohary, M.S. Elkotamy, H.A. Abdel-Aziz, Molecular docking, DFT and antiproliferative properties of 4-(3, 4-dimethoxyphenyl)-3-(4-methoxyphenyl)-1-phenyl-1H-pyrazolo [3, 4-b] pyridine as potent anticancer agent with CDK2 and PIM1 inhibition potency, *Drug Development Research* 85(7) (2024) e70009.
- [57] N.A. Alshaye, M.K. Elgohary, M.S. Elkotamy, H.A. Abdel-Aziz, Design, Synthesis and Biological Assessment of N'-(2-Oxoindolin-3-ylidene)-6-methylimidazo [2, 1-b] thiazole-5-carbohydrazides as Potential Anti-Proliferative Agents toward MCF-7 Breast Cancer, *Pharmaceuticals* 17(2) (2024) 216.
- [58] M.K. Elgohary, M.S. Elkotamy, S.T. Al-Rashood, F.A. Binjubair, R.S. Alarifi, H.A. Ghabbour, W.M. Eldehna, H.A. Abdel-Aziz, Exploring antitumor activity of novel imidazo [2, 1-b] thiazole and imidazo [1, 2-a] pyridine derivatives on MDA-MB-231 cell line: Targeting VEGFR-2 enzyme with computational insight, *Journal of Molecular Structure* 1322 (2025) 140579.
- [59] J. Brognard, T. Hunter, Protein kinase signaling networks in cancer, *Current opinion in genetics & development* 21(1) (2011) 4-11.
- [60] B. Chen, J. Lai, D. Dai, R. Chen, X. Li, N. Liao, JAK1 as a prognostic marker and its correlation with immune infiltrates in breast cancer, *Aging (Albany NY)* 11(23) (2019) 11124.